
Article:
Jian, W., Liang, D., Shao, S. et al. (2 more authors) (2015) SPH study of the evolution of water–water interfaces in dam break flows. Natural Hazards. ISSN 0921-030X

https://doi.org/10.1007/s11069-015-1726-6

SPH Study of the Evolution of Water-Water Interfaces in Dam Break Flows

Wei Jian[1], Dongfang Liang[2], Songdong Shao[3], Ridong Chen[4] and Xingnian Liu[5]

[1] Department of Engineering, University of Cambridge, Cambridge CB2 1PZ, UK. Email: wjian229@gmail.com

[2] Department of Engineering, University of Cambridge, Cambridge CB2 1PZ, UK. Email: dl359@cam.ac.uk

[3] Department of Civil and Structural Engineering, University of Sheffield, Sheffield S1 3JD, UK (State Key Laboratory of Hydro-Science and Engineering, Tsinghua University, Beijing 100084, China). Email: s.shao@sheffield.ac.uk (Author of Correspondence)

[4] State Key Laboratory of Hydraulics and Mountain River Engineering, Sichuan University, Chengdu 610065, China. Email: chenridong1984@163.com

[5] State Key Laboratory of Hydraulics and Mountain River Engineering, Sichuan University, Chengdu 610065, China. Email: scucrs@163.com

Abstract

The mixing process of upstream and downstream waters in the dam break flow could generate significant ecological impact on the downstream reaches and influence the environmental damages caused by the dam break flood. This is not easily investigated with the analytical and numerical models based on the grid method due to the large deformation of free surface and the water-water interface. In this paper, a weakly compressible Smoothed Particle Hydrodynamics (WCSPH) solver is used to study the advection and mixing process of the water bodies in two-dimensional dam-break flows over a wet bed. The numerical results of the mixing dynamics immediately after the release of the dam water are found to agree satisfactorily with the published experimental and numerical results. Then further investigations are carried out to study the interface development at the later stage of dam-break flows in a long channel. The analyses concentrate on the evolution of the interface at different ratios between the upstream and downstream water depths. The potential capabilities of the mesh-free SPH modelling approach for predicting the detailed development of the water-water interfaces are fully demonstrated.

Keywords: SPH; dam break; mixing; interface

1. Introduction

For free-surface flows, the Smoothed Particle Hydrodynamics (SPH) technique proves to be a promising numerical method in modelling large surface deformations and moving interfaces, even with the presence of water fragmentation and coalescence. Its particle nature provides a straightforward tool for handling complex and moving geometries, since the fluid motion can be easily traced using the Lagrangian description. The SPH method was initially proposed for the astrophysical applications. Lucy (1977) and Gingold and Monaghan (1977) independently modified the Particle-in-Cell (PIC) method to derive a pure particle treatment for the pressure and velocity fields. The particles are linked with each other by a kernel function. Monaghan first extended the SPH application to model incompressible flows with a free surface (1994), in which a weakly compressible assumption was made to model the fluid incompressibility without further computational complication, and an equation of state was used to couple the density and pressure fields. Later studies on the method have extended the application to a variety of hydrodynamic problems. Researches on the surface wave movement, interfacial flow and fluid–structure interaction have demonstrated promising capabilities of the SPH method (e.g. Dalrymple and Rogers, 2006; Violeau and Issa, 2007). In general, it is considered that the SPH method has a great potential for analysing flows involving large deformation, free surface, moving interface, deformable boundary and moving discontinuity.

Dam-break flows involve the formation of shocks, which arise from the step changes in the initial water level. Under the shallow water assumption, there exist analytical solutions to the problem. However, these may not accurately reflect the actual situations especially in the early stage of the dam break flow, when the large vertical acceleration invalidates the basic foundation of the Shallow Water Equations (SWEs) (Liang, 2010). In recent years, the emphasis of research has shifted to the development of Navier-Stokes (N-S) solvers for the dam-break flows, which have also become a widely used benchmark in the study of the rapid and interfacial flows. Due to its Lagrangian description, the SPH method has been successfully applied to dam-break flows in both two- and three-dimensional configurations. Monaghan (1994) studied a simple dam-break flow to demonstrate the capability of the model. Gómez-Gesteira and Dalrymple (2004) reproduced the impact of the flood wave on a

tall structure using a three-dimensional SPH model. The water surface evolutions over dry and wet beds were also analyzed and compared with the experimental data by Crespo (2008) and Crespo et al. (2008). Khayyer and Gotoh (2010) investigated similar problems by using two different mesh-free particle modelling approaches (i.e. MPS/SPH) and evaluated their improved schemes. The major objective of their work is to highlight the potential capabilities of the improved particle numerical schemes in reproducing the detailed features of complicated hydrodynamics. However, their study only focused on the early stage of the dam break flow mixing process and thus the channel length is relatively short. Although very detailed physical mechanisms of dam break flow mixing process have been investigated by Crepso et al. (2008), such as the energy dissipation and vorticity generation, the study is limited by the small spatial and temporal scales of the laboratory test. In addition, Lee et al. (2010) used a three-dimensional WCSPH model to study spillway hydraulics in a practical situation. Furthermore, the two-phase water-sediment mixture interface in a dam break flow was studied by Shakibaeinia and Jin (2011), and water-air interface issue was addressed by Colagrossi and Landrini (2003). More advanced SPH modelling of dam break flows based on the SWEs are attributed to Chang et al. (2011) and Kao and Chang (2012).

Compared with the pure hydrodynamic studies, the mixing of upstream and downstream waters in dam break flows has been less well understood. The study of dam-break flow mixing process has both theoretical and practical importance in water engineering due to its relevance to the ecological and environmental damages caused by the floods, and the understanding of this process could lead to a better water management and improve the hydro-environmental status of the water system. This paper attempts to numerically model such a mixing process, especially the evolution of the interface between the upstream and downstream waters. As shock waves are always associated with the dam break flows which involve large deformation of free surface and flow interface, the mixing process is a challenge to the traditional analytical and numerical approaches. In this paper, the mesh-free SPH method is applied to the dam-break flow predictions with an emphasis on the associated mixing process. The SPH technique is a mesh-free Lagrangian modelling approach. Its robustness lies in its ability to track the free surfaces and multi-interfaces in an easy and straightforward manner, thus it is well-suited for the study of dam break flow mixing and interface development. The grid modelling techniques solve the hydrodynamic equations on a

fixed grid system, thus numerical diffusion and complicated mesh re-configurations are unavoidable when treating the multi-interfaces. In addition, by comparing the numerical solutions with the experimental results, the pros and cons of other alternative numerical approaches for predicting such rapidly varied flows are highlighted.

2. SPH Methodology and Implementation

This section provides a detailed overview of the methodology and implementation of the weakly compressible SPH method, namely the WCSPH method. The SPH formulation is based on the concept of integral interpolations. Using a kernel function to relate the movement of the fluid particles, differential operators in the Navier-Stokes equations can be approximated by summations over the discrete particles. Each particle carries information about the velocity, density, mass, pressure and other flow variables over time (Monaghan, 1994).

In SPH, the approximation of any function $f(\mathbf{r})$ at particle i can be written in terms of the values at neighbouring particles within a compact support zone in the following notation:

$$f(\mathbf{r}_i) \approx \sum_j \frac{m_j}{\rho_j} f(\mathbf{r}_j) W_{ij} \tag{1}$$

where m_j, ρ_j denote the mass and density of the neighbouring particle j, respectively; $\mathbf{r}_j$ is the spatial position of the particle j and W_{ij} represents the kernel function between particle i and j, $W(\mathbf{r}_i - \mathbf{r}_j, h)$, where h is the smoothing length. As in many hydrodynamic computations, the kernel function used here is the Cubic Spline kernel function. It is a third-order polynomial with a compact support based on a family of spline functions. The smoothing length is often taken to be $h = 1.0 \sim 1.3\Delta r$, where Δr is the initial fluid particle spacing.

The particle approximation for the spatial derivative of a function can be written with regard to the kernel function as

$$\nabla f(\mathbf{r}_i) \approx \sum_j \frac{m_j}{\rho_j} f(\mathbf{r}_j) \nabla_i W_{ij} \tag{2}$$

where $\nabla_i W_{ij}$ denotes the gradient of the kernel function with respect to particle i.

To model incompressible flows, the associated fluid is assumed to be weakly compressible in order to minimise the computational complication. The continuity equation for a weakly compressible fluid takes the following form:

$$\frac{d\rho}{dt} = -\rho \nabla \cdot \mathbf{v} \tag{3}$$

where t is the time and **v** is the velocity vector field. The SPH form of the continuity equation can therefore be derived as:

$$\frac{d\rho_i}{dt} = -\rho_i \sum_j \frac{m_j}{\rho_j} (\mathbf{v}_j - \mathbf{v}_i) \cdot \nabla_i W_{ij} \tag{4}$$

The momentum equation for a weakly compressible fluid reads:

$$\frac{d\mathbf{v}}{dt} = -\frac{1}{\rho} \nabla P + \nu \nabla^2 \mathbf{v} + \mathbf{F} \tag{5}$$

where ν is the viscosity coefficient; P is the pressure and **F** is the external body force.

In practice, the pressure gradient is often computed in the following form:

$$\nabla P(\mathbf{r}_i) \approx \rho_i \sum_j m_j \left(\frac{P(\mathbf{r}_i)}{\rho_i^2} + \frac{P(\mathbf{r}_j)}{\rho_j^2} \right) \nabla_i W_{ij} \tag{6}$$

Viscosity is important in improving the stability of the simulation. Instead of discretising the viscosity term in Equation (5), the artificial viscosity often used in the WCSPH is proposed by Monaghan (1994) as follows:

$$\Pi_{ij} = \begin{cases} \dfrac{-\alpha \overline{c_{ij}} \mu_{ij} + \beta \mu_{ij}^2}{\overline{\rho_{ij}}} & \mathbf{v}_{ij} \cdot \mathbf{r}_{ij} < 0 \\ 0 & \mathbf{v}_{ij} \cdot \mathbf{r}_{ij} > 0 \end{cases} \tag{7}$$

where $\mu_{ij} = \dfrac{h \mathbf{v}_{ij} \cdot \mathbf{r}_{ij}}{\mathbf{r}_{ij}^2 + \eta^2}$ and the relevant notations can be found in Monaghan (1994). α is the bulk viscosity and β is the Von Neumann-Richtmyer viscosity. The latter is taken to be zero in present applications. The artificial viscosity term is introduced to allow for the presence of

121 shocks and to avoid the particle interpenetration, but the disadvantage is that it may lead to
122 unphysical decay and diffusion of vorticity in some strong shear flows. Crespo et al. (2008)
123 adopted a value of coefficient α = 0.08 for the dam break mixing flows and it was later
124 found by Khayyer and Gotoh (2010) that the simulations could lead to excessive vorticity
125 dissipation. They obtained more stable results when decreasing the coefficient from 0.08 to
126 0.02. By balancing the viscous decay and the integrity of free surface profiles, a value of 0.02
127 was used for all the applications presented in this paper.
128
129 In order to close the equation systems, an equation of state has been adopted to relate the
130 pressure to the density. For water it takes the following form

131 $$P = B\left(\left(\frac{\rho}{\rho_0}\right)^{\gamma} - 1\right) \tag{8}$$

132 where ρ_0 is the reference density that is usually set to 1000.0 kg/m^3 for water; and γ is a
133 constant that is normally taken to be 7. The parameter B sets a maximum limit for the density
134 variation allowed in the flow. It is calculated based on $c_0^2\rho_0/\gamma$, where c_0 is the speed of
135 sound at the reference density.
136
137 The particle positions are updated using the velocity calculated from the momentum equation.
138 In practical computations, the following XSPH variant is used to increase the numerical
139 stability and accuracy

140 $$\frac{d\mathbf{r}_i}{dt} = \mathbf{v}_i - \varepsilon\sum_j \frac{m_j}{\rho_j}\mathbf{v}_{ij}W_{ij} \tag{9}$$

141 where ε is a constant in the range between 0.0 and 1.0 depending on the application. In this
142 paper, ε is taken as 0.5 following Crespo et al. (2008). In most dam break flow simulations,
143 ε has been taken to be around 0.5 to achieve the best performances (Monaghan, 1994).
144 However, we should realize that the increase of this value may lead to more numerical
145 smoothing effect, so attentions should be paid to calibrate the optimum value for small
146 amplitude waves.

147

The time integration procedures of the continuity and momentum equations follow the modified predictor-corrector Euler scheme (Monaghan, 1994). Owing to the large sound speed required for the weakly compressible assumption, very small time step is needed in the WCSPH model to satisfy the CFL condition. In this paper, all of the WCSPH computations are based on an in-house code developed in Liang (2010) and Liang et al. (2010).

The initial setting of the particle positions plays an important role in the accuracy and computational efficiency of the SPH method. In WCSPH, a common practise is to first conduct a numerical simulation under the hydrostatic condition until the movement of particles becomes very small, and then the actual dynamic simulation starts. On the solid boundaries, the non-penetration condition must be satisfied. In the present work, the Lennards-Jones repulsive force method is used in the WCSPH model for its simplicity and effectiveness. On the free surface, both kinematic and dynamic boundary conditions can be automatically met by the Lagrangian nature of the SPH method.

It has been noticed that the summation interpolant fails to reproduce a constant function in some actual simulations, which often leads to unphysical variation of the local density field especially near the boundaries. In the WCSPH model used in this work, the Shephard filtering is performed every 40 time steps to reinitialize the density field. Hence, the numerical stability is maintained. One of the major instabilities experienced by the SPH model is the particle clumping in certain simulations. Monaghan (2000) introduced an additional term, f_{ij}, into the momentum equation to exert a repulsive force between the fluid particles with small separations. This force is dependent on the kernel function and the pressure field, which takes the form of

$$f_{ij} = 0.01\left(\frac{P_i}{\rho_i^2} + \frac{P_j}{\rho_j^2}\right)\left(\frac{W_{ij}}{W(\Delta r)}\right)^n \tag{10}$$

where $W(\Delta r)$ is the kernel function value based on the initial particle spacing; and n is a constant normally set at 4. Finally, the momentum equation (5) in SPH form becomes

$$\frac{d\mathbf{v}_i}{dt} = -\sum_j m_j\left(\frac{P_i}{\rho_i^2} + \frac{P_j}{\rho_j^2} + \Pi_{ij} + f_{ij}\right)\nabla_i W_{ij} + \mathbf{g} \tag{11}$$

where the external force term includes the gravitational acceleration $\mathbf{g}$ only.

3. Model Validations: Dam-break Flow Propagation

In this section, the propagation of a dam-break flow is simulated and validated against the experimental work detailed in Stansby et al. (1998), the analytical solutions to the Shallow Water Equations and the numerical solutions to the Navier-Stokes equations using the Volume of Fluid (VOF) method (Jian, 2013), in which FLUENT13.0 is used and thus the numerical scheme is based on the Finite Volume method. The test case considers the instantaneous collapse of a dam in a wide, horizontal and frictionless channel of 200 m long. Water is initially static and separated by a gate located at x = 100 m. The initial conditions are defined as:

$$u(x,0) = 0, \quad h(x,0) = \begin{cases} h_1 & \text{if } x > 100\,\text{m} \\ h_0 & \text{if } x \le 100\,\text{m} \end{cases} \tag{12}$$

where h_0 is the initial water depth upstream of the dam; and h_1 is the initial water depth in the downstream channel. In this study, the upstream water depth h_0 is kept constant at 10.0 m, while three different values have been considered for h_1: 0.0 m for a dry bed, 1.0 m for a shallow wet bed, and 4.5 m for a deep wet bed, respectively.

The parameters used in the WCSPH model are: initial particle spacing Δr = 0.1 m and time step Δt = 0.0002 s. In the grid-based VOF model, the main computational parameters are: grid size of 0.1 × 0.1 m^2 and time step Δt = 0.005 s. Hence, the spatial resolutions of the mesh-free and grid-based models are comparable.

3.1 Results and discussions

Figures 1 to 3 illustrate the comparisons among the numerical results of the WCSPH model, the experimental data of Stansby et al. (2008), analytical solutions to the SWEs (Jian, 2013) and numerical solutions to the Navier-Stokes equations using the VOF method (Jian, 2013), with the initial downstream water depths being h_1 = 0.0 m, 1.0 m and 4.5 m, respectively.

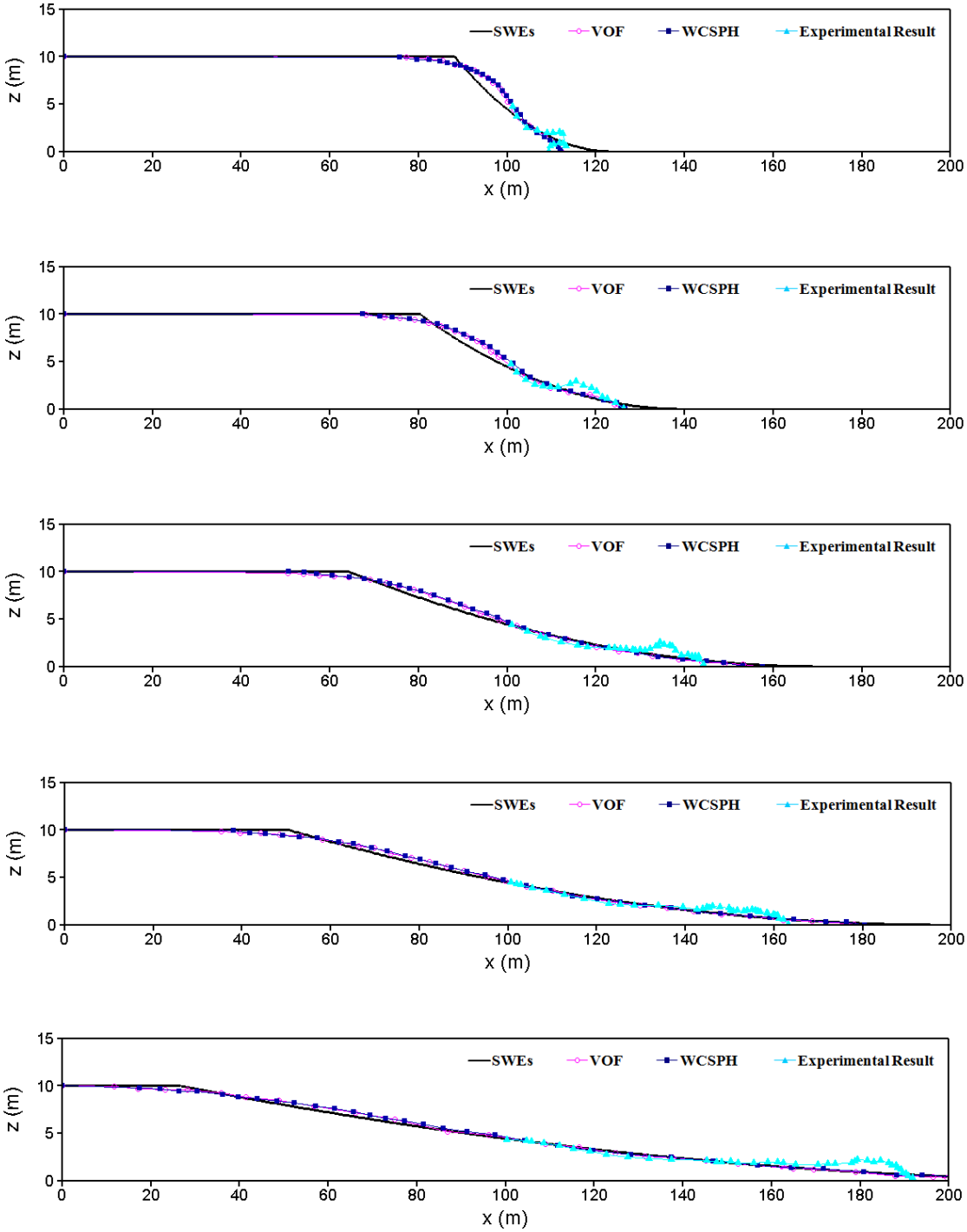

Figure 1 Free surface profiles in the dam-break flow over dry bed h_1 = 0.0 m, at t = 1.20 s, 2.00 s, 3.60 s, 5.00 s and 7.40 s, respectively

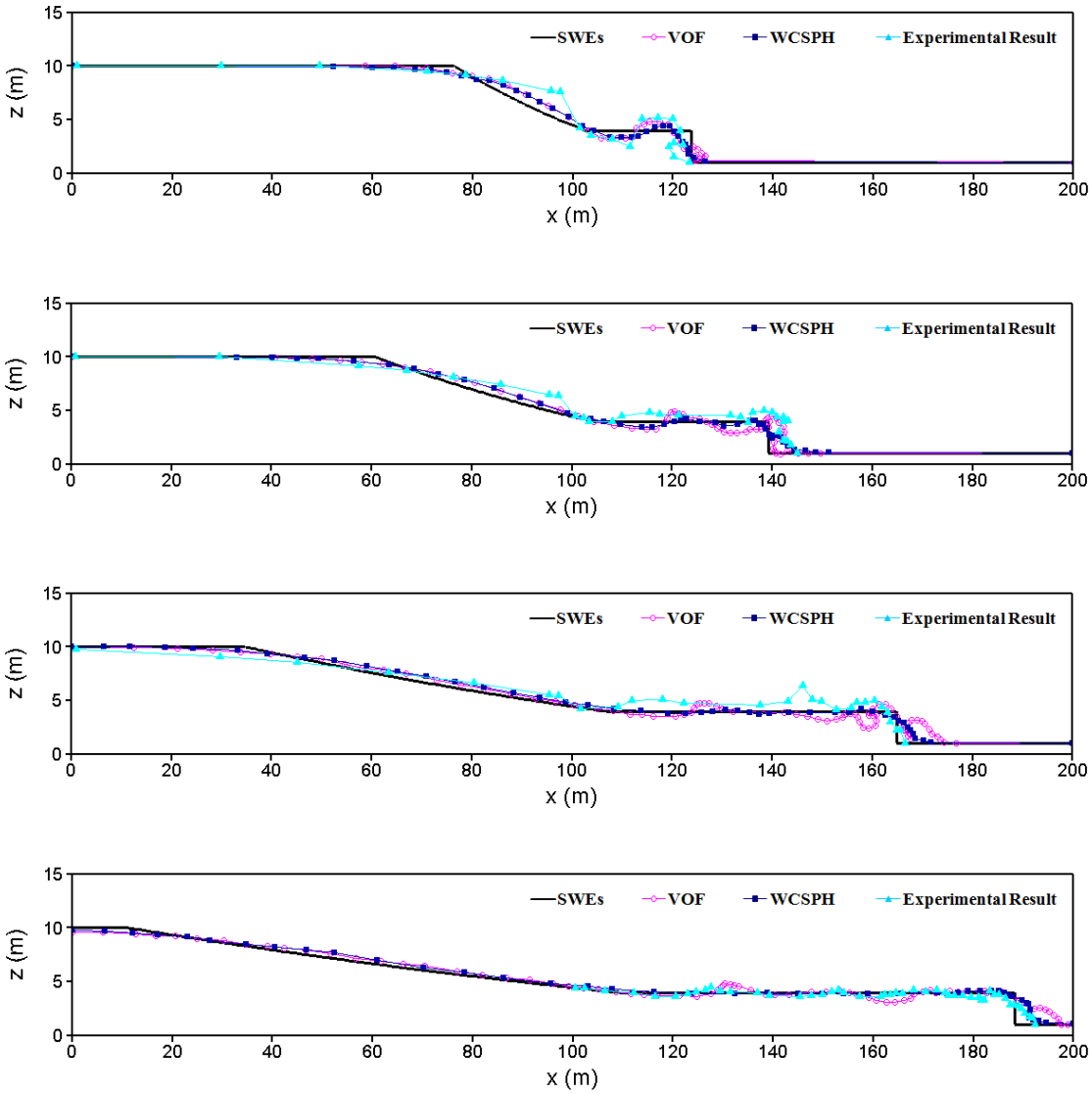

Figure 2 Free surface profiles in the dam-break flow over shallow wet bed h_1 = 1.0 m, at t = 2.40 s, 4.00 s, 6.60 s and 9.00 s, respectively

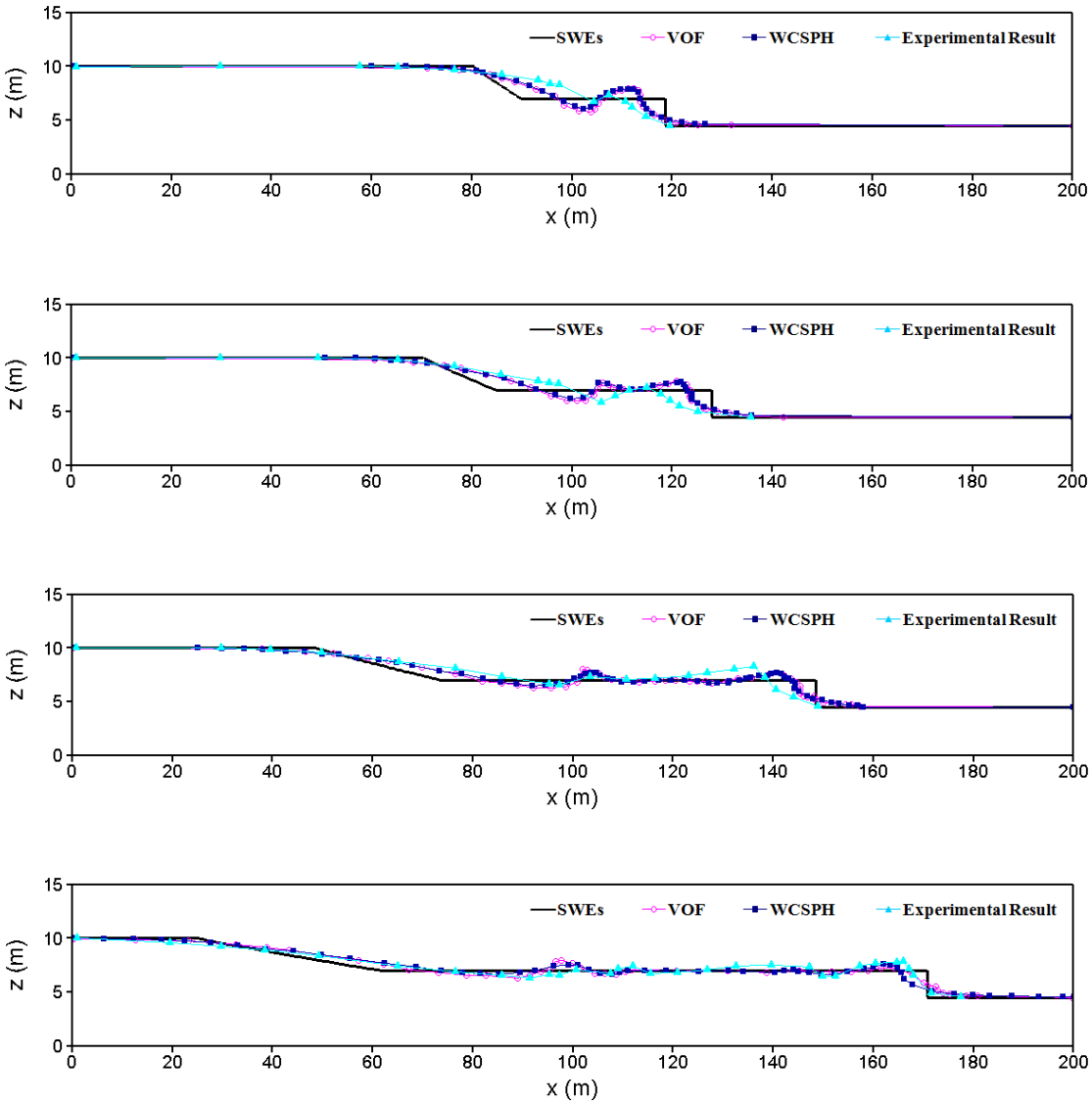

Figure 3 Free surface profiles in the dam-break flow over deep wet bed h_1 = 4.5 m, at t = 2.00 s, 3.00 s, 5.20 s and 7.60 s, respectively

It is seen from Figures 1 to 3 that the flow caused by the collapsed dam behaves very differently depending on the downstream depths. For a dry bed, the forward momentum dominates the fluid movement and the flood front is established very quickly. Figure 1 shows that, by t = 1.20 s, the wave front has already settled into a stable form and its propagation for the rest of simulation is free of any breaking. If there is initially a layer of water in the downstream channel, the upstream water can build up into the front with a significant height. A mushroom-like waveform emerges in both Figures 2 and 3 immediately after the dam collapses. The downstream condition generally determines the shape of the wave front that propagates downstream. If the initial downstream water depth is shallow, the accumulated water front soon breaks onto the static water in the channel, driven by the large pressure gradient as shown in the surface profile at t = 6.60 s in Figure 2. The broken wave front continues to travel downstream, accompanied by some small-scale breakings at the interface between the reservoir water and the channel water. The overall waveform under the shallow water layer condition is characterised by the water front travelling downstream. This is, however, not the case in the deep downstream water condition as shown in Figure 3, in which the mushroom-like water front seen at t = 2.00 s gradually evolves into two distinct wave forms travelling in the opposite direction. The experimental data suggests that the downstream-propagating water front is slightly more prominent, whereas the numerical results indicate a more balanced strength between the two wave fronts.

All of the three scenarios observe a good agreement between the WCSPH and VOF computations against the experimental data. Both models are based on the Navier-Stokes equations and are able to predict the propagation of the dam-break flow with good accuracy. However, slight discrepancies exist in the propagation speed between the experimental observations and numerical predictions. Due to the assumption of frictionless solid boundaries, the propagation of the wave front is over-predicted under the dry bed condition. In addition, the numerical predictions tend to estimate a more rapid wave front development under the deep downstream water layer setting. For all three cases, the solutions to the SWEs deviate significantly from the experimental observations immediately after the dam collapse. This is because the SWEs are only able to provide approximate predictions of the free surface when there is insignificant variation in the vertical direction (Liang, 2010). Therefore, some of the key features observed in the experimental results are lost in the SWEs predictions.

Despite this, the propagation speed of the wave front agrees well with the experimental data, except that a slight over-estimation is found for the case of the deep ambient layer. Once the flow has settled into an established form at the later stage, the accuracy of the SWEs prediction improves significantly as the flow characteristics satisfy the underlying long-wave assumptions adopted in deriving the SWEs. Similar observations have also been reported in Pu et al. (2013).

One distinct advantage of the WCSPH model is its superior computational efficiency over the VOF model for the three cases considered here. Table 1 lists the CPU time required for simulating the cases using the WCSPH and VOF models. Since the VOF method needs to simulate the flow of both the water and air phases, it requires a significantly longer computational time.

Table 1 CPU time required for the dam-break flow simulations

Test case	Physical time (s)	CPU time (hr)	
		WCSPH	VOF
Dry bed (h_0 = 10.0 m and h_1 = 0.0 m)	7.40	3.10	11.30
Shallow wet bed (h_0 = 10.0 m and h_1 = 1.0 m)	9.00	4.08	14.15
Deep wet bed (h_0 = 10.0 m and h_1 = 4.5 m)	7.60	4.96	17.12

4. Model Application: Mixing Process in Near-field Dam-break Flows

From the model validations in the previous section, we understand that, in the case of a wet downstream bed, the collapsed water undergoes a dynamic interaction with the water body downstream, which incurs significant mechanical energy dissipation. This section pays particular attention to the mixing process involved in dam-break flows. Ignoring the

molecular diffusion, the mixing of the water bodies can be considered as the non-uniform advection of the water associated with the violent wave movements. Here, we apply the WCSPH model to focus on the mixing process involved in the early stage of dam-break flows. The numerical results are compared with the published experimental results. We need to mention that no advanced turbulence closures are included in the WCSPH model, except the artificial viscosity mentioned before. The term of near-field indicates the mixing process situation immediately after the dam break when the interface between the reservoir water and tail water is very complicated.

4.1 Model setup and computational parameters

The validation case examines the interaction between two water bodies in a dam-break flow problem immediately after the release of the dammed water. The numerical study is based on the experiment in Janosi et al. (2004). Figure 4 shows the experimental setup of a two-dimensional flume with two compartments separated by a gate at x = 0.38 m. A volume of water with a height of 0.15 m (h_0) is initially locked up in the upstream compartment. The gate is gradually lifted up at a removal rate of approximately 1.5 m/s after the experiment starts, allowing the initially locked water to seep through the opening. Several different downstream depths are considered: shallow ambient layer with depth h_1 = 0.015 m and deep ambient layer with h_1 = 0.030 m, 0.058 m and 0.070 m, respectively.

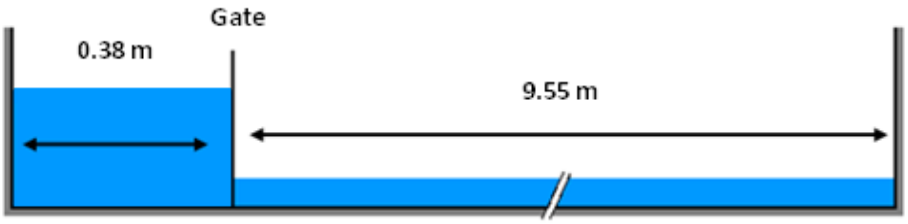

Figure 4 Experimental setup of the dam-break flow in Janosi et al. (2004)

To increase computational efficiency, a shorter computational domain was adopted in the model. Since the physical time of interest is 0.6 seconds in total, the downstream channel

length can be reduced to 2.5 m without affecting the results. In the SPH computations, the initial particle spacing is Δr = 0.001 m in the shallow depth condition and 0.002 m in the deep depth condition. The corresponding time steps are $\Delta t = 1.0\times10^{-5}$ s and 2.0×10^{-5} s, respectively. The gate is modelled by a set of repulsive particles, with their positions and velocities externally specified to resemble the removal procedure. The two water bodies are tracked by assigning different flags to the upstream and downstream water particles at the beginning of the simulation so that the mixing interface can be identified as the separation of the particles carrying different flags.

4.2 Results and discussions for the shallow ambient layer

The WCSPH results and the experimental observations (Janosi et al., 2004) are compared in Figure 5 for the case of the shallow ambient layer depth h_1 = 0.015 m. It is evident that the numerical model is able to reproduce the wave propagation after the gradual removal of the gate. The main features observed in the experimental snapshots, such as the formation of a mushroom-like water jet and the subsequent wave breakings, are resembled in the numerical predictions with reasonable accuracy. There are some discrepancies in the mixing profiles between the experimental and numerical results. The mixing interface observed during the experiment remains relatively vertical throughout the time with only a slight sloping towards the downstream direction at t = 0.392 s. In addition, the profiles at t = 0.327 s and 0.392 s suggest that the plunging wave front is mostly composed of channel water. The numerically predicted interfaces exhibit varying degrees of inclination towards the downstream in their mixing profiles. However, the overall agreement is still satisfactory.

Another key feature observed in the mixing patterns is the presence of a thin layer of downstream water at the surface upstream of the plunging water front. That water is brought to the surface by an up-thrust movement during the initial collision of the two water bodies. The WCSPH model is able to capture the presence and development of this thin water layer.

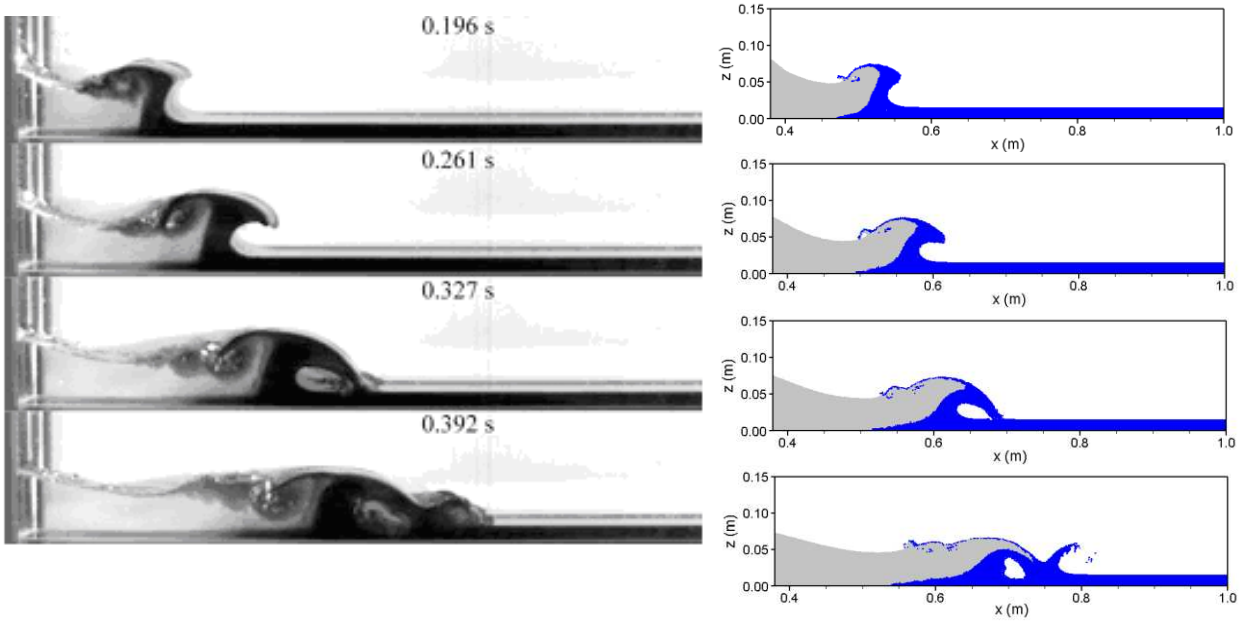

Figure 5 Experimental (left, Janosi et al., 2004) and numerical (right) mixing patterns at t = 0.196 s, 0.261 s, 0.327 s and 0.392 s for shallow flow depth h_1 = 0.015 m

4.3 Results and discussions for the deep ambient layers

Three large downstream flow depths have been analysed, i.e. h_1 = 0.030 m, 0.058 m and 0.070 m. Figure 6 presents the experimental snapshots and numerical predictions of the mixing patterns at t = 0.30 s. It is shown that with the increased downstream water depth, the collision between the two water bodies and the subsequent breaking exhibit quite different characteristics from those shown in the shallow ambient layer condition.

With h_1 = 0.030 m, the wave front shows an established mushroom-like shape at t = 0.30 s. The formation of the waveform is slower when compared with the case in Figure 5 for the shallow layer. Generally speaking, the SPH simulations show a satisfactory agreement with the experimental results at t = 0.30 s. The discrepancy lies in the amount of downstream water at the surface. The experimental snapshot suggests that the downstream water makes up approximately half of the plunging wave column, whereas the numerical prediction only shows a relatively thin layer at the free surface which is similar to the case of the shallow ambient layer. Figure 6 also shows that the waveforms take longer time to fully develop with increasing downstream water depth. The experimental snapshots for h_1 = 0.058 m and 0.070

m suggest that the wave fronts are still gaining their height at this instant. In addition, the corresponding mixing interfaces take different shapes to the ones studied previously. It closely resembles a straight line for h_1 = 0.058 m, while inclines slightly towards the upstream direction with h_1 = 0.070 m. Again, the WCSPH model demonstrates a good estimation of the mixing feature at the free surface. Consistent with the case for h_1 = 0.030 m, the model underestimates the amount of mixing upstream of the wave front.

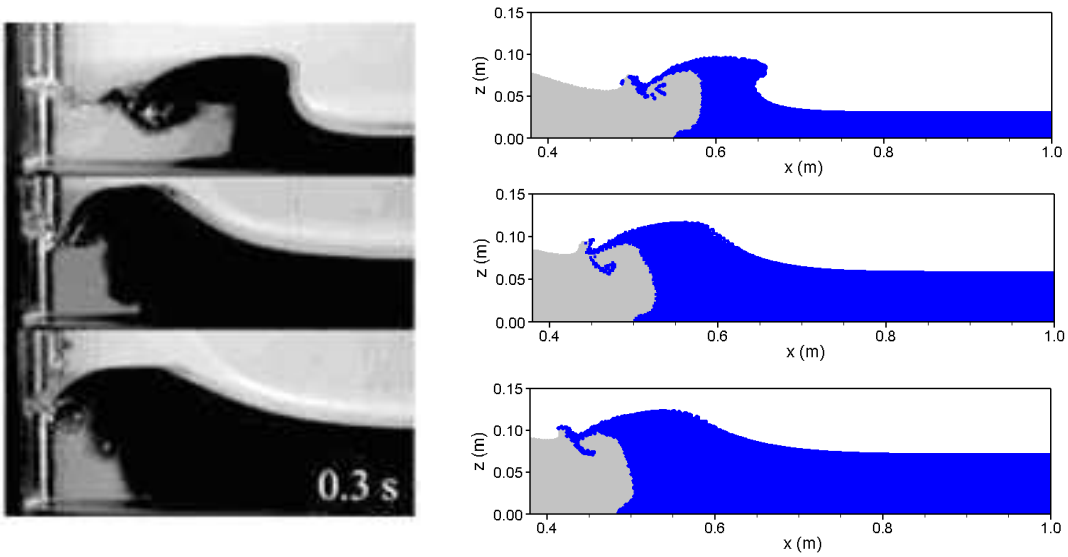

Figure 6 Experimental (left Jonasi et al., 2004) and numerical (right) mixing patterns at t = 0.3 s for h_1 = 0.030 m (top), 0.058 m (middle) and 0.070 m (bottom)

As the wave front travels further downstream, the mixing interface evolves into patterns that are considerably different from the characteristics seen in the early stage. Figure 7 shows the experimental snapshots and the corresponding SPH simulations at t = 0.60 s. The mixing interfaces are now located at quite some distance upstream of the propagating wave front. The numerical model can still crudely reproduce the mixing dynamics at this time. Figure 7 displays mixing interfaces inclining slightly upstream near the free surface. Except for a thin boundary layer immediately above the bed, the upstream water appears to advance faster close to the bottom. Another difference from the early-stage mixing as shown in Figure 6 is that the two water bodies are relatively well mixed by this time. Similar numerical

simulations have also been carried out using the VOF method (Jian and Liang, 2012), which found that the WCSPH model is computationally more efficient than the VOF model for all the depths considered.

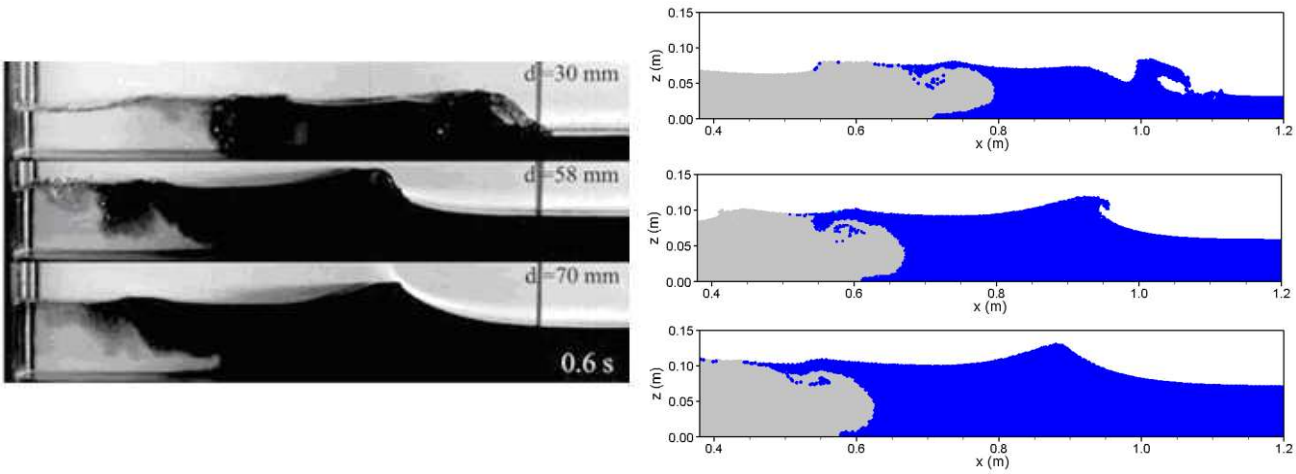

Figure 7 Experimental (left Jonasi et al., 2004) and numerical (right) mixing patterns at t = 0.6 s for h_1 = 0.030 m (top), 0.058 m (middle) and 0.070 m (bottom)

5. Model Application: Dam Break Flow Mixing in a Long Channel

In this section, the WCSPH model is applied to study the interface development of dam break flow in a long channel. We will focus on the later stage of the mixing process, when the interface becomes less chaotic. Immediately after the dam-break, there is a violent mixing between the reservoir water and tail water due to the formation of the vortices. The later stage is when these violent vortical motions settle down after the flood front has travelled some distance downstream. At this stage, the interface between different water regions is quite clear, and can be approximated by using a straight line. The study would be useful for evaluating the hydro-environment in long waterways. The bores in the waterways can be formed by not only the dam breaks but also tides and tsunamis.

5.1 Model setup and computational parameters

The numerical setup of this hypothetical dam-break problem consists of a 2000 m long horizontal water tank. Water is initially stagnant and separated by a gate located at $x = 1000$ m. The initial conditions are thus defined as:

$$u(x,0) = 0, \quad h(x,0) = \begin{cases} h_1 & \text{if } x > 1000\,\text{m} \\ h_0 & \text{if } x \le 1000\,\text{m} \end{cases} \tag{13}$$

The initial upstream water depth h_0 is set at 10.0 m throughout the study. Several downstream water depths have been investigated, ranging from 2.0 m ~ 7.0 m. As a reference, the analytical solution to the SWEs (Jian, 2013) is included to evaluate the predictions of dam break wave propagations and the corresponding mixing process.

In the WCSPH model, a particle size of 0.2 m is used for the best compromise between the computational efficiency and accuracy. The total simulation time is 50.0 s, which ensures that the wave front even under the smallest depth ratio does not reach the downstream end of the channel. The computational time step is $\Delta t = 0.0004$ s.

5.2 Discussion on the flow field

The numerical results of the WCSPH model are compared with the analytical solutions to the SWEs. It has been well known that the SWEs model is capable of producing reasonable estimations of the wave propagation at the later stage of dam-break flows when there is less variation in the vertical direction. Three downstream water depths (h_1) are considered for the validation purpose: h_1 = 2.00 m, 5.00 m and 7.00 m. The simulations aim to test the shallow water assumptions and provide a full picture of the wave propagations over the shallow, medium and deep water depths.

For the smallest downstream water depth h_1 = 2.00 m, the WCSPH results agree extremely well with the solutions to the SWEs in terms of the surface profiles as shown in Figure 8. However, when the downstream water depths increase to h_1 = 5.0 m and 7.0 m, the wave propagations predicted by the WCSPH model in Figures 9 and 10 fall behind the analytical predictions according to the SWEs. It is also shown that this difference in the propagation speed increases with time and the downstream water depth.

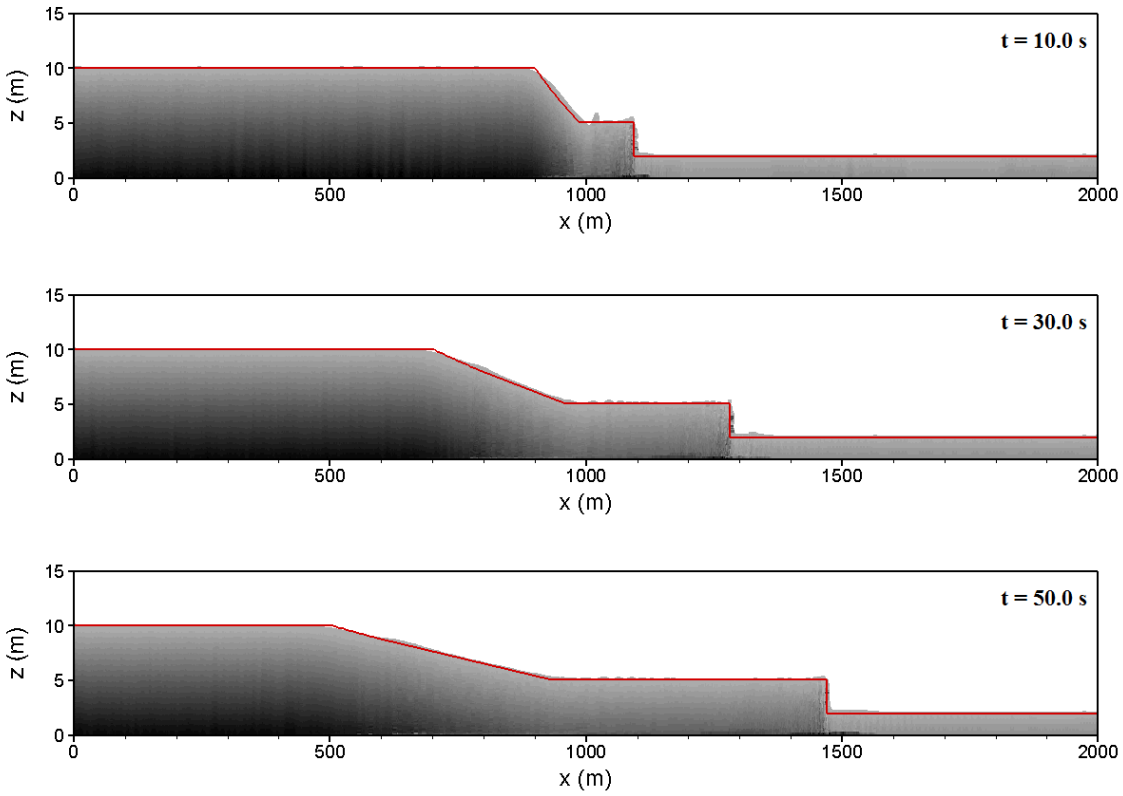

Figure 8 Analytical solutions (solid line) and WCSPH results (shaded area) of surface profiles at t = 10.0 s, 30.0 s and 50.0 s for h_0 = 10.0 m and h_1 = 2.0 m

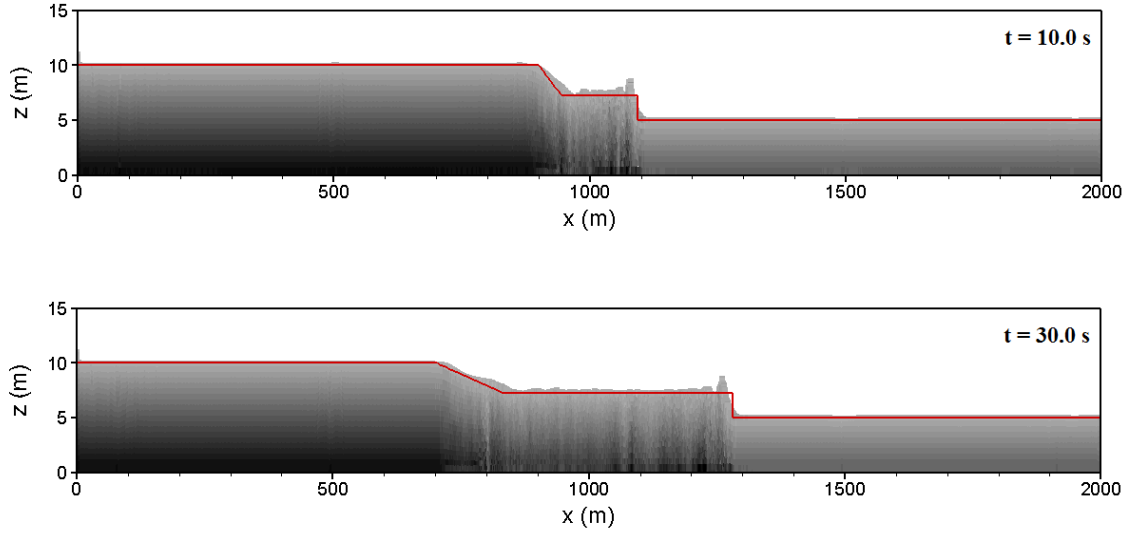

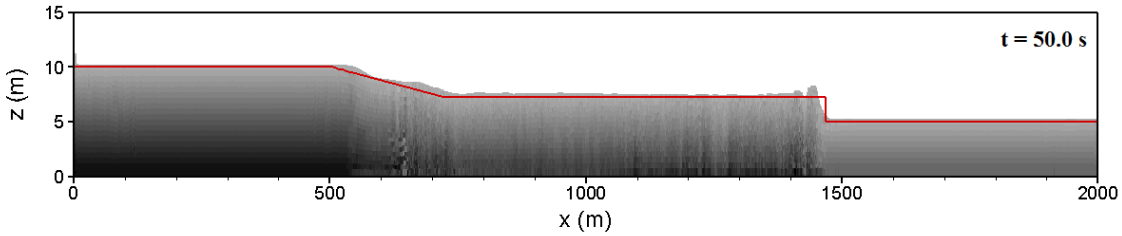

Figure 9 Analytical solutions (solid line) and WCSPH results (shaded area) of surface profiles at t = 10.0 s, 30.0 s and 50.0 s for h_0 = 10.0 m and h_1 = 5.0 m

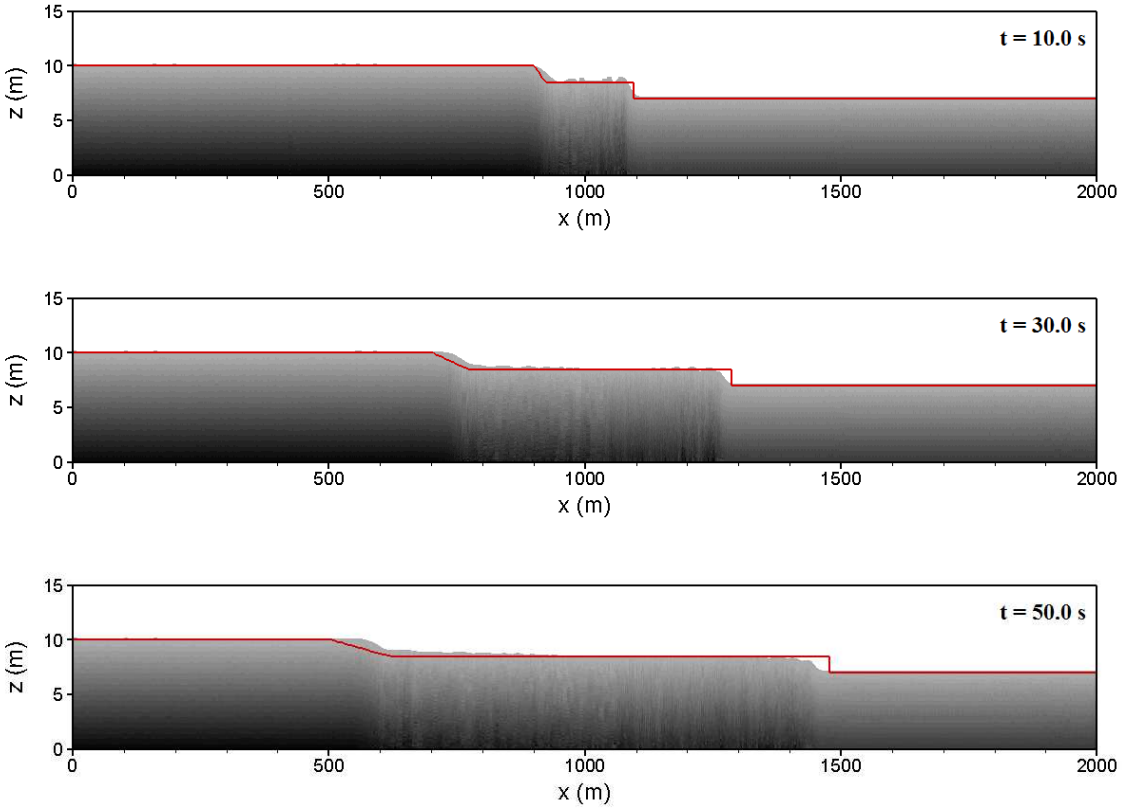

Figure 10 Analytical solutions (solid line) and WCSPH results (shaded area) of surface profiles at t = 10.0 s, 30.0 s and 50.0 s for h_0 = 10.0 m and h_1 = 7.0 m

The situations in Figures 8 to 10 are consistent with the horizontal velocity distributions of the three downstream flow depths computed at t = 50.0 s, as shown in Figure 11. The average velocity predicted by the WCSPH model agrees well with the SWEs prediction at h_1

= 2.0 m, but is 3.3% smaller at h_1 = 5.0 m and 25% smaller at h_1 = 7.0 m. The discrepancy is thought to be caused mainly by the over-estimation of fluid bulk speed arisen from the uniform velocity distribution over the depth in the SWEs. In the previous validation case, the solutions to the SWEs also tend to give a faster propagation at the deep downstream water layer when compared with experimental observations. The VOF modelling results in Jian (2013) also confirms the accuracy of the present WCSPH computations.

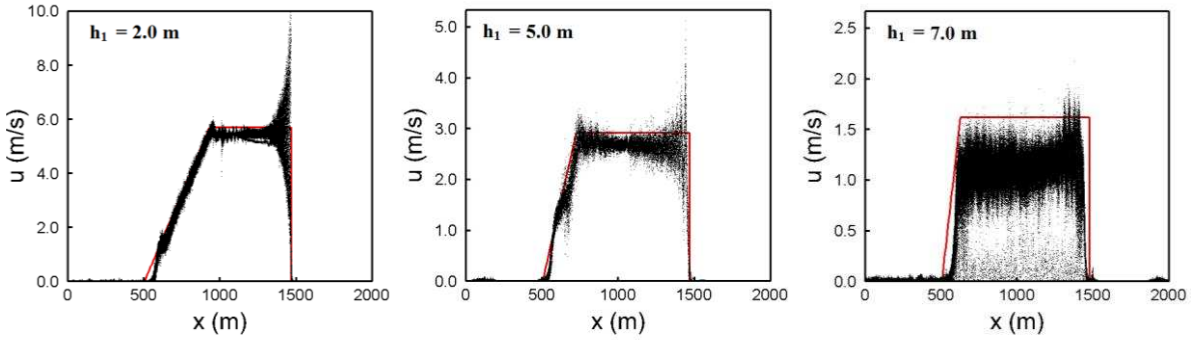

Figure 11 Analytical solutions (solid line) and WCSPH results (dot) of the velocity distribution at t = 50.0 s for h_1 = 2.0 m, 5.0 m and 7.0 m

Here we need to point out that Figures 8 to 10 show some kinds of oscillations around the wave front in the SPH results while these are not found in the analytic solutions of SWEs. Due to the assumption of hydrostatic pressure distribution in the SWEs, the SWEs model always generates a step wave front without numerical dispersion. The refinement of the SWEs by adding the Boussinesq terms could demonstrate much more satisfactory performance in the case of rapidly varied flows such as dam break in an open channel, which was reported in the latest SPH applications in the field (Chang et al., 2014).

5.3 Discussion on the mixing

Disregarding the chemical reaction and molecular diffusion between the upstream and downstream waters, the mixing interface can be determined solely by the advection of fluid particles. Here, the evolution of mixing dynamics is analysed with regard to the interface evolution over the time and the influence of the water depth ratios.

Figure 12 presents the mixing profiles from t = 5.0 s to 50.0 s for the downstream depth h_1 = 3.0 m and the corresponding horizontal velocity profiles are shown in Figure 13 (sloped lines in the velocity figures indicate the location of interface between the reservoir water and tail water). The early surface profiles indicate that the waveforms have already settled into some well-established propagating fronts, with little wave breaking across the flow field. The velocity profile at t = 0.0004 s shows a large gradient in the horizontal velocity field along the initial discontinuity. This reflects the large momentum exerted by the collapsed water on the stagnant downstream flow. The velocity gradient causes the vertically positioned interface to slowly evolve into an inclined slope. By the time t = 5.0 s, the surface profile indicates that the interface has already developed into a curve with a larger steepness near the free surface. The velocity profile at t = 5.0 s still exhibits a large velocity gradient over the depth. The magnitude within the immediate mixing zone is approximately less than 4.0 m/s at the lower part of the water depth and over 4.5 m/s at the upper part. This drives the mixing interface to incline further downstream. By t = 10.0 s, the interface becomes more inclined, mainly driven by the fast-moving fluid particles above the mid-depth. The velocity gradient has reduced by at least 0.3 m/s across the depth in the mixing zone that envelops the interface. From t = 10.0 s to 20.0 s, the velocity gradient within the mixing zone has further reduced by approximately 0.2 m/s. Most of the fast-moving particles seen at t = 10.0 s have slowed down. Only a small number of them are still visible within 1.0 m beneath the free surface in the velocity profile at t = 20.0 s. Beyond t = 20.0 s, the mixing interface seems to settle into a relatively stable shape. Little change is observed in the mixing interface from t = 20.0 s to 50.0 s. The slope of the interface is approximately 32° above the mid-depth while the lower part remains at around 20°. The velocity fields indicate that the flow domain has settled at a horizontal velocity of around 4.4 m/s for the rest of the simulation.

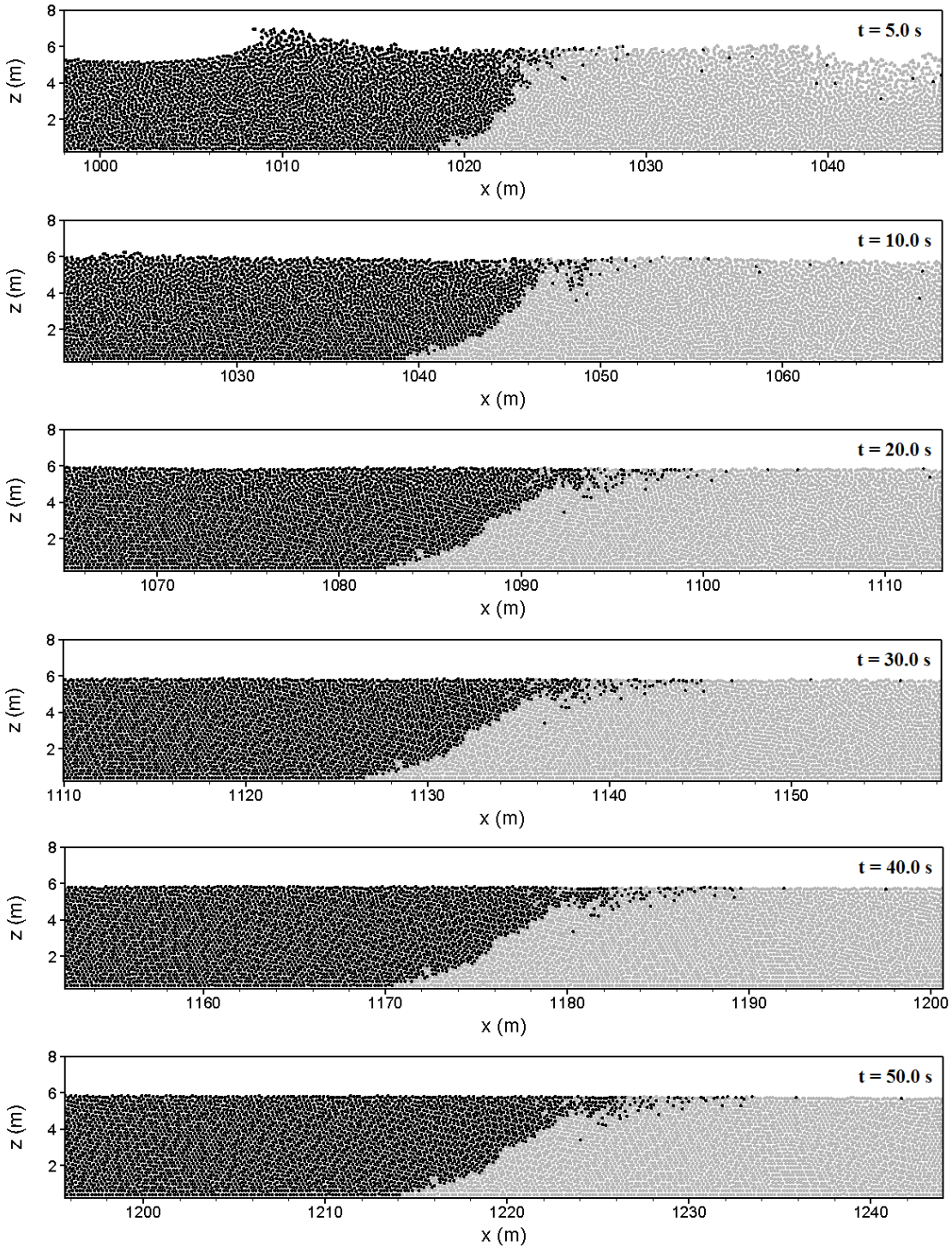

Figure 12 Mixing patterns for downstream water depth h_1 = 3.0 m at t = 5.0 s, 10.0 s, 20.0 s, 30.0 s, 40.0 s and 50.0 s

602
603
604
605
606
607
608
609

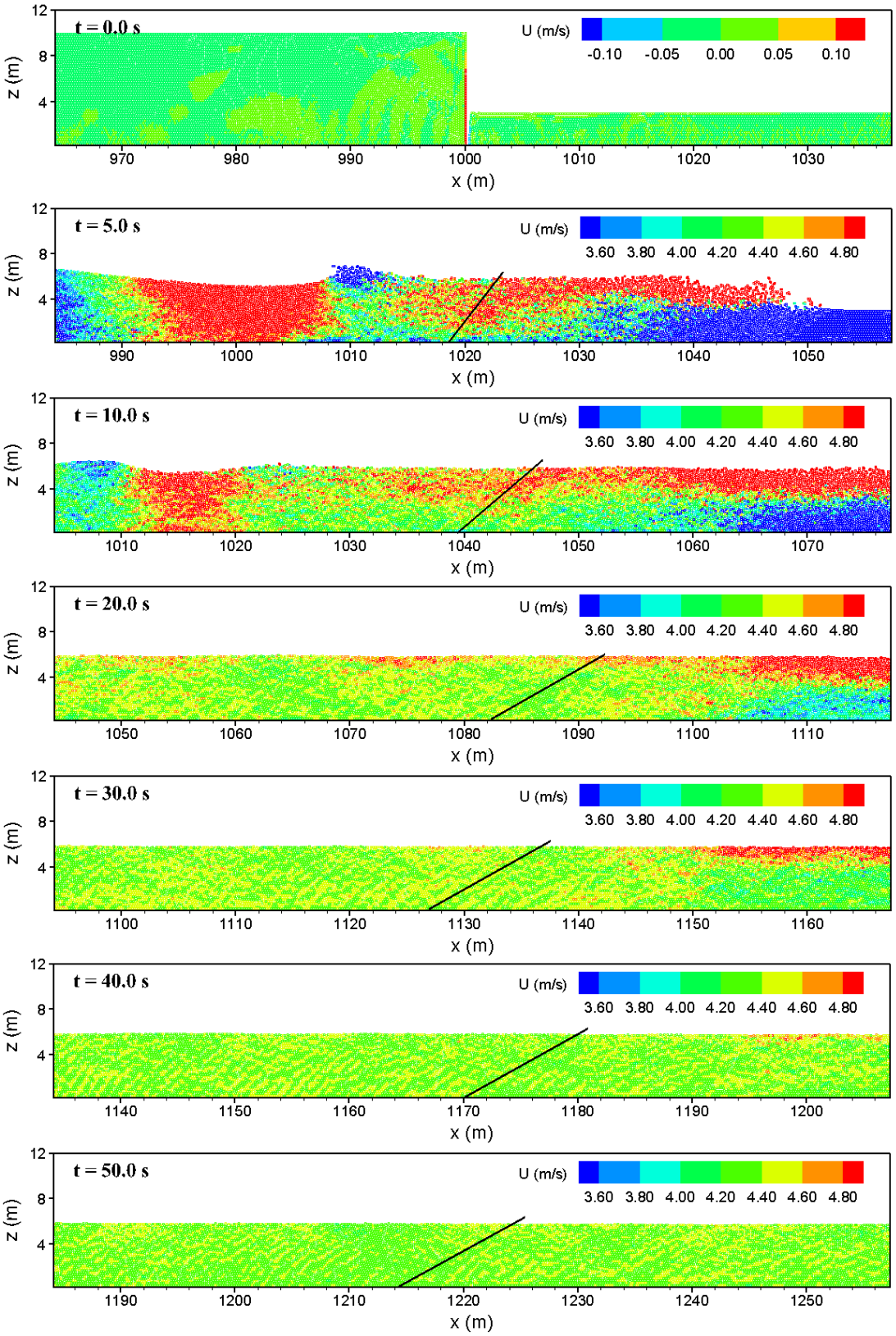

610 **Figure 13 Horizontal velocity distributions for downstream water depth h_1 = 3.0 m at t**

611 **= 0.0004 s, 5.0 s, 10.0 s, 20.0 s, 30.0 s, 40.0 s and 50.0 s**

612 Similar features of the interface evolution and velocity distribution can also be observed at a
613 larger downstream water depth h_1 = 6.0 m. Owing to the larger pressure force and inertia
614 effect of the downstream water body, the interfaces are much steeper than the small depth
615 case at all instants. However, the mixing process still settles into a stable state within the
616 immediate mixing zone by t = 20.0 s. The horizontal velocity settles at an equilibrium value
617 of approximately 2.1 m/s beyond t = 20.0 s. There is little change to the interfacial curves
618 after this time. The detailed results are not plotted in this paper to save space, but interested
619 readers are referred to Jian (2013).
620
621 In summary, the interfaces all take the shape of a forward-leaning line a certain period after
622 the initiation of the dam-break. The mixing interface developments for a range of
623 downstream water depths, varying from h_1 = 2.0 m to 7.0 m, are tracked over the time and
624 plotted in Figure 14. The x-axis shows the span of the mixing curve from its most upstream
625 point near the bottom of the channel to its most downstream point at the free surface. In order
626 to minimise the complication at the bottom boundary, the interfaces are tracked from a
627 distance equivalent to one particle size above the solid boundary. Figure 14 shows the
628 evidence that the equilibrium state is reached by t = 20.0 s for most of the depth ratios. Very
629 little change in the interface shapes takes place after this time, except for h_1 = 7.0 m, where
630 small adjustments can be found at the later time. All interfaces at t = 10.0 s demonstrate a
631 change in the slope of the interface above the mid-depth. The lower part of the interfaces
632 undergoes only slight adjustment in the process of reaching their equilibrium forms,
633 especially for h_1 > 5.0 m. Most of the changes occur near the free surface, where fluid
634 particles take longer time to slow down. The horizontal span of the mixing interface
635 decreases with the increasing depth ratio (h_1 / h_0), and a larger h_1 / h_0 also corresponds to the
636 faster establishment of the final equilibrium state. These can be explained by the influence of
637 the horizontal velocity gradient in the vertical direction, since a larger downstream water
638 depth gives rise to smaller velocity non-uniformity over the water column. Generally
639 speaking, the mixing dynamics are significantly affected by the horizontal velocity gradient
640 over the water depth. There are no further changes in the interface curve when the
641 equilibrium state is reached in the horizontal velocity field.
642

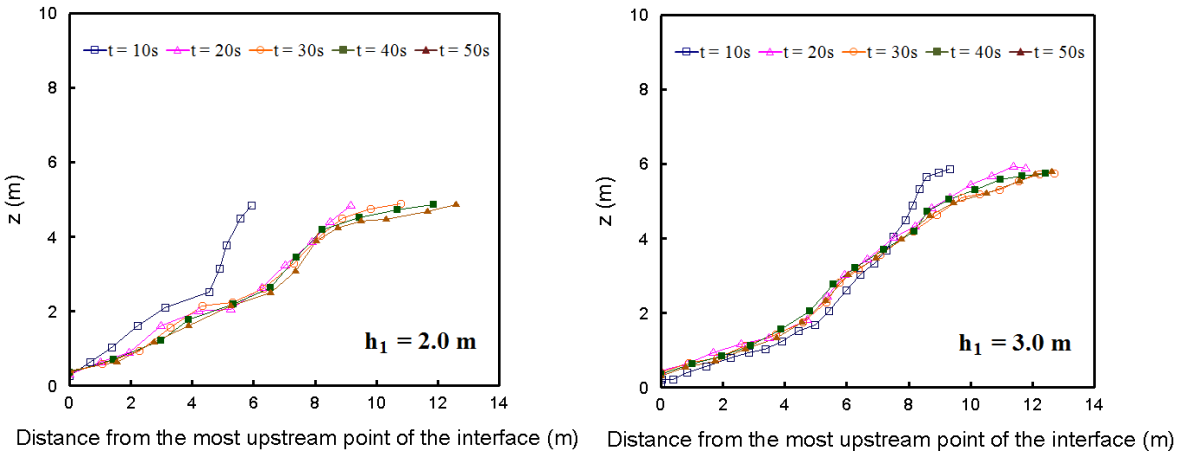

643
644

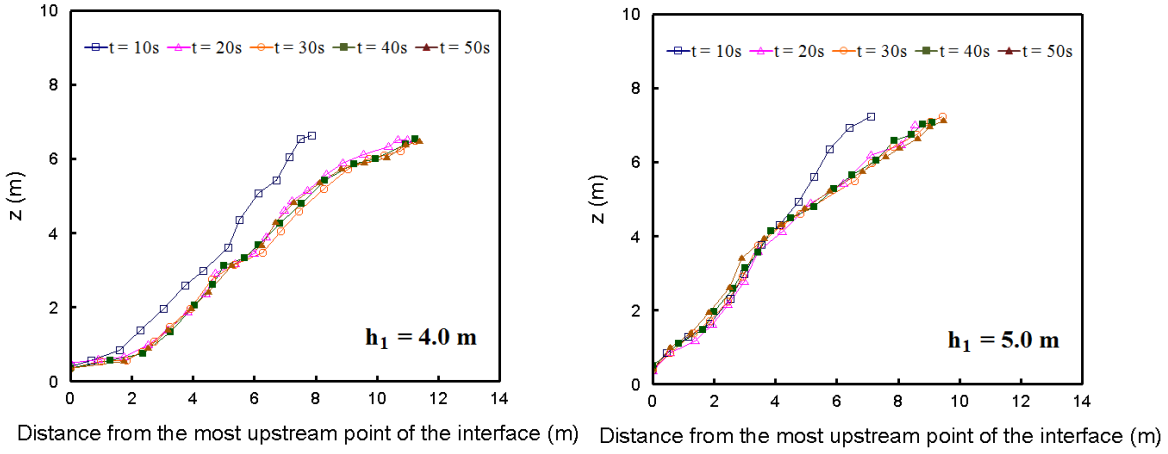

645

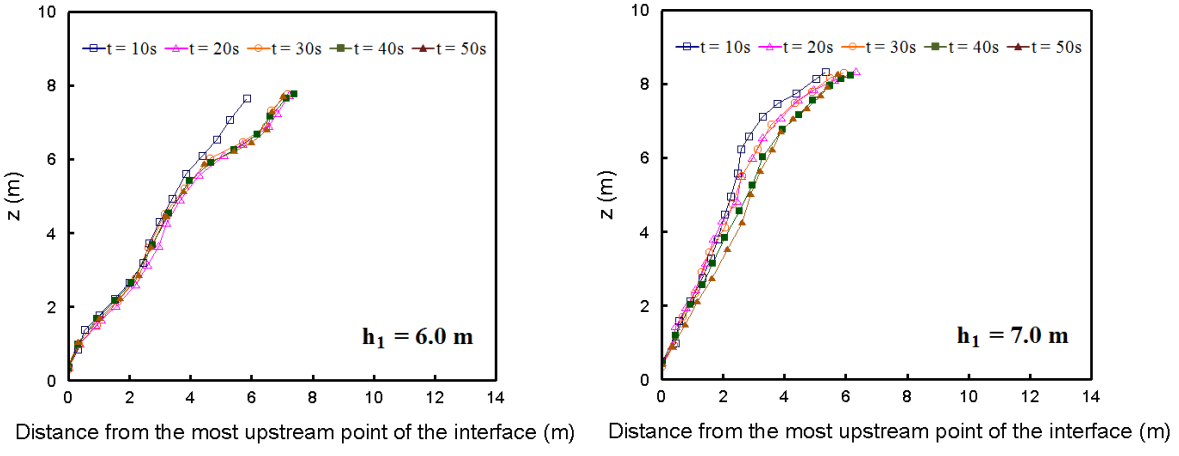

646
647

648 **Figure 14 Mixing interface developments for h_1 = 2.0 m ~ 7.0 m**

649

650

5.4 Fully established mixing interface and its dependence on the depth ratio

The discussions in the previous section suggest that the initial depth ratio plays an important role in the mixing dynamics in dam-break flows. This section further studies the effect of the initial depth ratios on the final mixing interface at the equilibrium state. Figure 15 shows the mixing profiles at t = 50.0 s for different downstream water depth ratios (h_1/h_0). It is evident that the slope of the mixing interface at the equilibrium state is positively correlated to the initial ratio between the downstream and upstream water depths. As discussed earlier, the final forms of the interface are generally determined by the horizontal velocity distributions in the first 20 seconds of the simulation. Figure 16 details the velocity fields of the mixing zone containing the interface for different depth ratios at t = 10.0 s. Reading from the scales of the velocity fields as indicated in the legends, it is evident that the magnitude of the velocity gradient decreases with the increasing depth ratio. As a result, the interface reaches the equilibrium state much faster and the slope of the corresponding interface profile is also expected to be steeper for the deep downstream water depth.

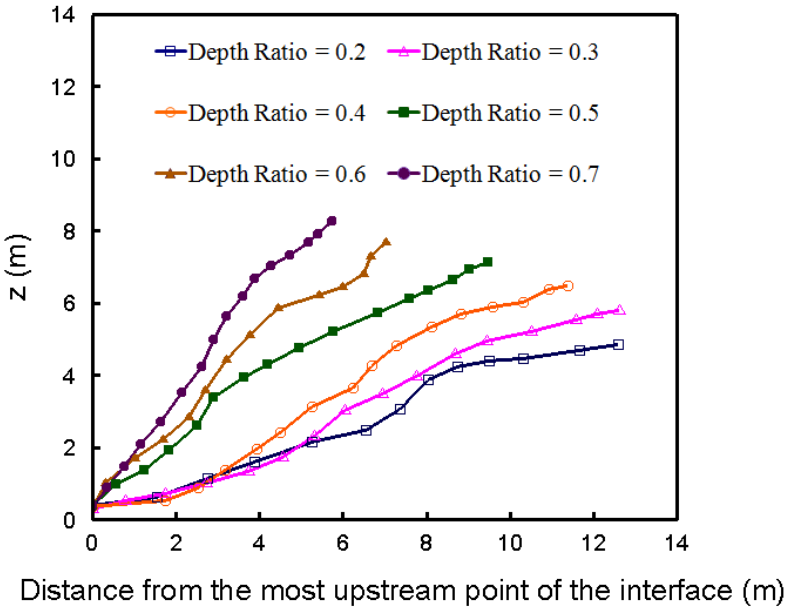

Figure 15 Mixing interface profiles for different depth ratios at t = 50.0 s

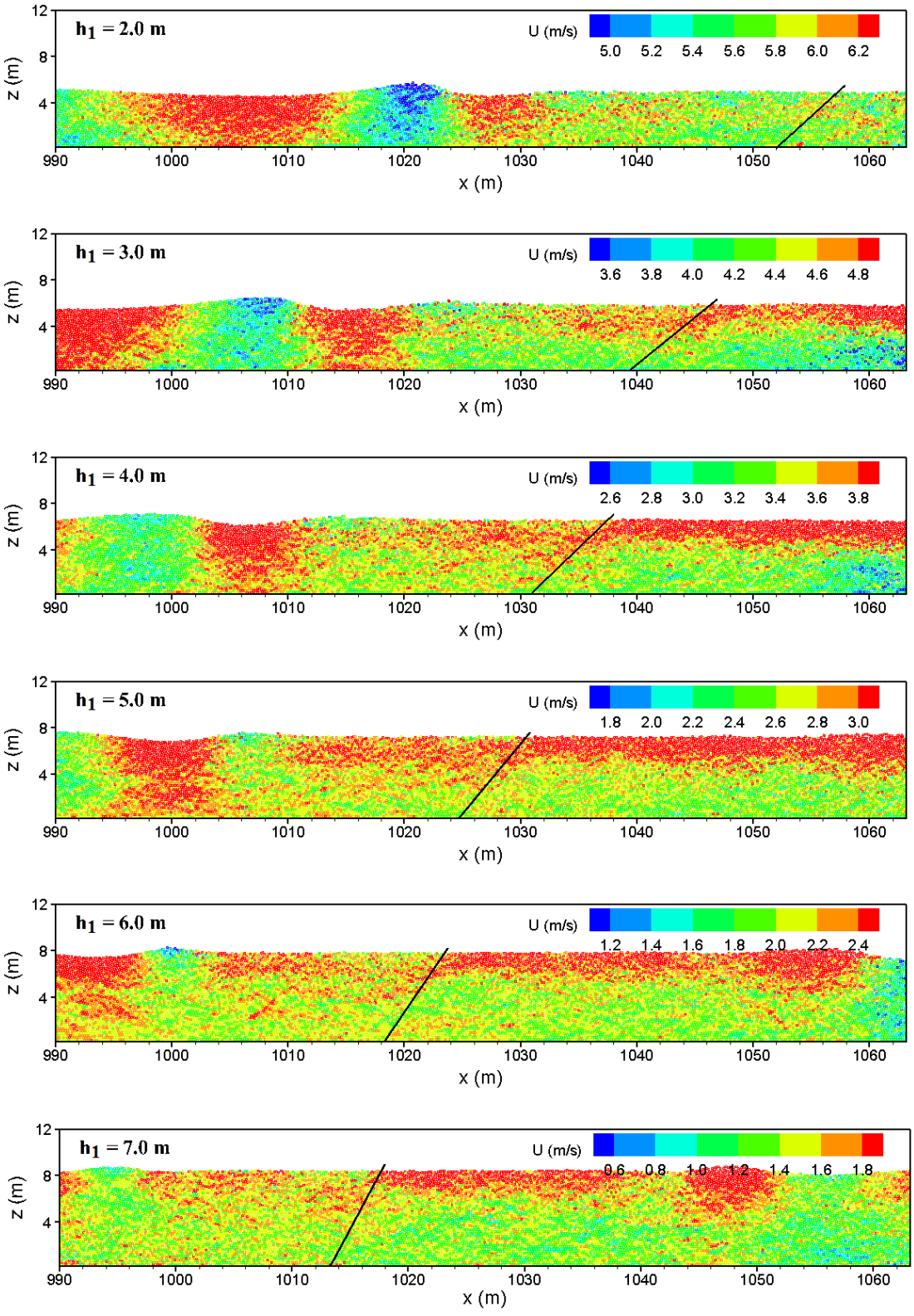

Figure 16 Horizontal velocity profiles for different depth ratios at t = 10.0 s

Each of the mixing interface profile in final steady state in Figure 15 can be normalised using the water depth of the mixing zone in the vertical direction and using the span of the interface in the horizontal direction. The normalized curves are plotted in Figure 17, which shows consistently similar forms regardless of the initial depth ratios. The overall angle of the slopes is approximately 45°. There exists a slight change of the slope at 20% of the water depth below the water surface. The slope of the interface becomes milder above this height.

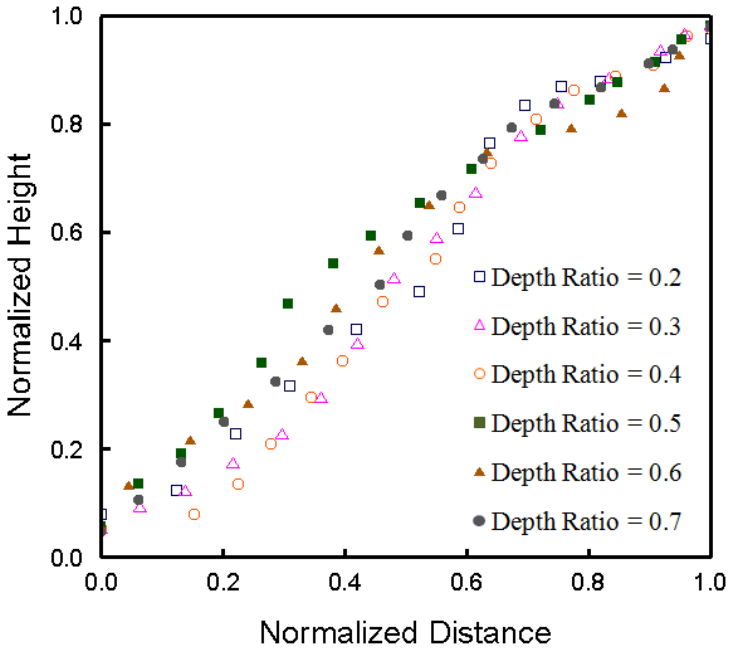

Figure 17 Normalized mixing interface curves for different depth ratios in equilibrium

6. Conclusions

This paper reports on the mixing process involved in both early and later stages of the dam-break flows, using the WCSPH simulations and the analytical solutions to the SWEs. A case study concerning dam-break flow propagation is first carried out to validate the WCSPH model, highlighting its capability of reproducing the surface profiles under different flow

conditions. The results from the model agree well with the experimental measurements, analytical solutions to the SWEs and numerical predictions based on the VOF model. Then the mixing process involved in dam-break flows is examined for the period immediately after the gate opening. The performance of the WCSPH model is validated against the experimental results for the near-field dam-break problem, proving its ability of simulating the mixing dynamics with satisfactory accuracy for both the shallow and deep ambient water layers.

The subsequent application pays attention to the mixing dynamics and the water-water interface development at the later stage of dam-break flow in a long water tank of 2000 m. Six different water depth ratios have been considered in the study. The SWEs tend to predict a faster propagation of the interface, particularly for the larger depth ratios, but they agree well with the WCSPH simulations in the shallow downstream water condition. The numerical results of the WCSPH model show that for all the depth ratios considered, the equilibrium state is reached by approximately t = 20.0 s after the instantaneous release. The interface curvature and velocity gradient remain largely unchanged afterwards. The numerical outcomes suggest that the interface develops into a curved slope soon after the simulation starts, driven by the gradient in the horizontal velocity field over the depth. As time elapses, the interface becomes more gradual near the surface as the fluid particles in the mid-depth region slow down more rapidly than the ones at the water surface. The slope of the mixing interface at the equilibrium state becomes steeper with the increasing downstream water depth.

As for the future research direction, it is recognised that the three-dimensional model is necessary to be able to reproduce a more realistic mixing process in dam break flows in a narrow channel where the side-wall effect is strong and the bed topography is complex.

Acknowledgements

The first author acknowledges the Jafar Studentship during her PhD study at the University of Cambridge. The other authors acknowledge the support of the

Major State Basic Research Development Program (973) of China (No. 2013CB036402), Open Fund of the State Key Laboratory of Hydraulics and Mountain River Engineering, Sichuan University (SKHL1404; SKHL1409), Start-up Grant for the Young Teachers of Sichuan University (2014SCU11056) and National Science and Technology Support Plan (2012BAB0513B0).

References

Chang, T. J., Chang, K. H. and Kao, H. M. (2014), A new approach to model weakly nonhydrostatic shallow water flows in open channels with smoothed particle hydrodynamics, Journal of Hydrology, 519, 1010-1019.

Chang, T. J., Kao, H. M. and Chang, K. H. (2011), Numerical simulation of shallow-water dam break flows in open channels using smoothed particle hydrodynamics, Journal of Hydrology, 408, 78-90.

Colagrossi, A. and Landrini, M. (2003), Numerical simulation of interfacial flows by smoothed particle hydrodynamics, Journal of Computational Physics, 191(2), 448-475.

Crespo, A. J. C. (2008), Application of the Smoothed Particle Hydrodynamics Model SPHysics to Free-surface Hydrodynamics, Ph.D. thesis, Universidade de Vigo.

Crespo, A. J. C., Gómez-Gesteira, M. and Dalrymple, R. A. (2008), Modelling dam break behaviour over a wet bed by a SPH technique, Journal of Waterway, Port, Coastal and Ocean Engineering, 134(6), 313-320.

Dalrymple, R. A. and Rogers, B. D. (2006), Numerical modelling of water waves with the SPH method, Coastal Engineering, 53(2-3), 141-147.

768 Gingold, R. A. and Monaghan, J. J. (1977), Smoothed particle hydrodynamics: theory and
769 application to non-spherical stars, Royal Astronomical Society Monthly Notices, 181, 375-
770 389.
771
772 Gómez-Gesteira, M. and Dalrymple, R. A. (2004), Using a 3D SPH method for wave impact
773 on a tall structure, Journal of Waterway, Port, Coastal and Ocean Engineering, 130(2), 63-69.
774
775 Jánosi, I. M., Jan, D., Szabó, K. G. and Tél, T. (2004), Turbulent drag reduction in dam-break
776 flows, Experiments in Fluids, 37, 219-229.
777
778 Jian, W. (2013), Smoothed Particle Hydrodynamics Modelling of Dam-break Flows and
779 Wave-structure Interactions, Ph.D. thesis, The University of Cambridge.
780
781 Jian, W. and Liang, D. (2012), On simulating mixing process in dam-break flows,
782 Proceedings of 2nd IAHR Europe Conference, Munich, 27-29 June, 1-6.
783
784 Kao, H. M. and Chang, T. J. (2012), Numerical modeling of dambreak-induced flood and
785 inundation using smoothed particle hydrodynamics, Journal of Hydrology, 448, 232-244.
786
787 Khayyer, A. and Gotoh, H. (2010), On particle-based simulation of a dam break over a wet
788 bed, Journal of Hydraulic Research, 48(2), 238-249.
789
790 Lee, E.-S., Violeau, D., Issa, R. and Ploix, S. (2010), Application of weakly compressible and
791 truly incompressible SPH to 3-D water collapse in waterworks, Journal of Hydraulic
792 Research, 48(Extra Issue), 50-60.
793
794 Liang, D. (2010), Evaluating shallow water assumptions in dam-break flows, Proceedings of
795 the ICE – Water Management, 163(5), 227-237.
796
797 Liang, D., Thusyanthan, I., Madabhushi, S. P. G. and Tang, H. (2010), Modelling solitary
798 waves and its impact on coastal houses with SPH method, China Ocean Engineering,
799 24(2), 353-368.

Lucy, L. (1977), A numerical approach to the testing of fission hypothesis, The Astronomical Journal, 82(12), 1013–1024.

Monaghan, J. J. (1994), Simulating free surface flows with SPH, Journal of Computational Physics, 110, 399-406.

Monaghan, J. J. (2000), SPH without a tensile instability, Journal of Computational Physics, 159(2), 290-311.

Pu, J., Shao, S., Huang, Y. and Hussain, K. (2013), Evaluations of SWEs and SPH numerical modelling techniques for dam break flows, Engineering Applications of Computational Fluid Mechanics, 7(4), 544-563.

Shakibaeinia, A. and Jin, Y. C. (2011), A mesh-free particle model for simulation of mobile-bed dam break, Advances in Water Resources, 34(6), 794-807.

Stansby, P. K., Chegini, A. and Barnes, T. C. (1998), The initial stages of dam-break flow, Journal of Fluid Mechanics, 374, 407–424.

Violeau, D. and Issa, R. (2007), Numerical modelling of complex turbulent free surface flows with the SPH method: an overview, International Journal for Numerical Methods in Fluids, 53(2), 277–304.